Exploiting ^{20}Ne Isotopes for Precision Characterizations of Collectivity in Small Systems

Giuliano Giacalone,[1,*] Benjamin Bally,[2] Govert Nijs,[3] Shihang Shen,[4] Thomas Duguet,[5,6] Jean-Paul Ebran,[7,8] Serdar Elhatisari,[9,10] Mikael Frosini,[11] Timo A. Lähde,[12,13] Dean Lee,[14] Bing-Nan Lu,[15] Yuan-Zhuo Ma,[14] Ulf-G. Meißner,[10,16,17] Jacquelyn Noronha-Hostler,[18] Christopher Plumberg,[19] Tomás R. Rodríguez,[20] Robert Roth,[21,22] Wilke van der Schee,[3,23,24] and Vittorio Somà[5]

[1]*Institut für Theoretische Physik, Universität Heidelberg, Philosophenweg 16, 69120 Heidelberg, Germany*
[2]*ESNT, IRFU, CEA, Université Paris-Saclay, 91191 Gif-sur-Yvette, France*
[3]*Theoretical Physics Department, CERN, CH-1211 Genève 23, Switzerland*
[4]*Institute for Advanced Simulation and Institut für Kernphysik, Forschungszentrum Jülich, D-52425 Jülich, Germany*
[5]*IRFU, CEA, Université Paris-Saclay, 91191 Gif-sur-Yvette, France*
[6]*KU Leuven, Instituut voor Kern- en Stralingsfysica, 3001 Leuven, Belgium*
[7]*CEA, DAM, DIF, 91297 Arpajon, France*
[8]*Université Paris-Saclay, CEA, Laboratoire Matière en Conditions Extrêmes, 91680 Bruyères-le-Châtel, France*
[9]*Faculty of Natural Sciences and Engineering, Gaziantep Islam Science and Technology University, Gaziantep 27010, Turkey*
[10]*Helmholtz-Institut für Strahlen- und Kernphysik and Bethe Center for Theoretical Physics, Universität Bonn, D-53115 Bonn, Germany*
[11]*CEA, DES, IRESNE, DER, SPRC, LEPh, 13115 Saint-Paul-lez-Durance, France*
[12]*Institut für Kernphysik, Institute for Advanced Simulation and Jülich Center for Hadron Physics, Forschungszentrum Julich, D-52425 Jülich, Germany*
[13]*Center for Advanced Simulation and Analytics (CASA), Forschungszentrum Julich, D-52425 Jülich, Germany*
[14]*Facility for Rare Isotope Beams and Department of Physics and Astronomy, Michigan State University, East Lansing, Michigan 48824, USA*
[15]*Graduate School of China Academy of Engineering Physics, Beijing 100193, China*
[16]*Institute for Advanced Simulation, Institut für Kernphysik, and Julich Center for Hadron Physics, Forschungszentrum Jülich, D-52425 Jülich, Germany*
[17]*Tbilisi State University, 0186 Tbilisi, Georgia*
[18]*Illinois Center for Advanced Studies of the Universe, Department of Physics, University of Illinois at Urbana-Champaign, Urbana, Illinois 61801, USA*
[19]*Natural Science Division, Pepperdine University, Malibu, California 90263, USA*
[20]*Departamento de Estructura de la Materia, Física Térmica y Electrónica and IPARCOS, Universidad Complutense de Madrid, E-28040 Madrid, Spain*
[21]*Institut für Kernphysik, Technische Universität Darmstadt, 64289 Darmstadt, Germany*
[22]*Helmholtz Forschungsakademie Hessen für FAIR, GSI Helmholtzzentrum, 64289 Darmstadt, Germany*
[23]*Institute for Theoretical Physics, Utrecht University, 3584 CC Utrecht, The Netherlands*
[24]*NIKHEF, Amsterdam, The Netherlands*

(Received 20 February 2024; accepted 16 June 2025; published 2 July 2025)

Whether or not femto-scale droplets of quark-gluon plasma (QGP) are formed in so-called small systems at high-energy colliders is a pressing question in the phenomenology of the strong interaction. For proton-proton or proton-nucleus collisions the answer is inconclusive due to the large theoretical uncertainties plaguing the description of these processes. While upcoming data on collisions of ^{16}O nuclei may mitigate these uncertainties in the near future, here we demonstrate the unique possibilities offered by complementing $^{16}\mathrm{O}+{}^{16}\mathrm{O}$ data with collisions of ^{20}Ne ions. We couple both nuclear lattice effective field theory (NLEFT) and projected generator coordinate method (PGCM) *ab initio* descriptions of the structure of ^{20}Ne and ^{16}O to hydrodynamic simulations of $^{16}\mathrm{O}+{}^{16}\mathrm{O}$ and $^{20}\mathrm{Ne}+{}^{20}\mathrm{Ne}$ collisions at high energy. We isolate the imprints of the bowling-pin shape of ^{20}Ne on the collective flow of hadrons, which can be used to perform quantitative tests of the hydrodynamic QGP paradigm. In particular, we predict that the elliptic flow of $^{20}\mathrm{Ne}+{}^{20}\mathrm{Ne}$ collisions is enhanced by as much as $1.174(8)_{\mathrm{stat}}(31)_{\mathrm{syst}}$ for NLEFT and

*Contact author: giacalone@thphys.uni-heidelberg.de

$1.139(6)_{\text{stat}}(39)_{\text{syst}}$ for PGCM relative to $^{16}\text{O} + ^{16}\text{O}$ collisions for the 1% most central events. At the same time, theoretical uncertainties largely cancel when studying relative variations of observables between two systems. This demonstrates a method based on experiments with two light-ion species for precision characterizations of the collective dynamics and its emergence in a small system.

DOI: 10.1103/k8rb-jgvq

Introduction—A central motivation for the program of ultrarelativistic nuclear collisions is to access bulk properties of QCD matter that emerge in conditions similar to those found in the early Universe or in extreme astrophysical objects [1]. A prime example is the quark-gluon plasma (QGP), the hot phase of QCD matter that behaves like a near-perfect fluid [2] Hydrodynamic behavior is inferred from the harmonic spectrum of the azimuthal distributions of final-state hadrons [3],

$$\frac{dN_{\text{ch}}}{d\eta d^2\mathbf{p}} = \frac{dN_{\text{ch}}}{d\eta dp_T}\frac{1}{2\pi}\left(1 + 2\sum_{n=1}^{\infty} v_n \cos n(\phi - \phi_n)\right),$$

where $dN_{\text{ch}}/d\eta d^2\mathbf{p}$ is the charged hadron distribution differential in pseudorapidity, η, and transverse momentum, $\mathbf{p}$, with $p_T = |\mathbf{p}|$ and ϕ the azimuthal angle. The coefficients v_n quantify the anisotropic flow. In hydrodynamics, v_n arise as a response of the system created in the interaction region to the anisotropy of its geometry, as dictated by an emergent pressure-gradient force [4], the hallmark of hydrodynamic behavior. An elliptical deformation of the interaction region leads to elliptic flow, v_2, a triangular deformation to v_3, and so on [5].

Observations of anisotropic flow in small systems [6,7], such as proton-nucleus and proton-proton collisions, have triggered tremendous efforts investigating whether a QGP description is appropriate even in regimes where applying hydrodynamics becomes hard to justify [8,9]. Theoretical studies have either pushed hydrodynamic simulations to extreme situations [10–15], analyzed in detail the transition from kinetic theory to hydrodynamics [16–23], or studied the emergence of collectivity via other mechanisms [24]. Small systems pose, thus, a fundamental challenge rooted in the issue of the thermalization and hydrodynamization of QCD matter [25–29].

To advance our knowledge of small systems, one has to isolate in the experimental data information able to discriminate theoretical approaches. A breakthrough in this direction would be the identification of a correlation between the final-state anisotropy in momentum space (v_n) and the deformation of the initial-state geometry, supporting an underlying hydrodynamic-type scenario. This strategy has been pursued at the Relativistic Heavy Ion Collider (RHIC) in a system-geometry scan comparing $p^{197}\text{Au}$ and $d^{197}\text{Au}$ collisions at the same beam energy. Defining $v_2\{2\} \equiv \sqrt{\langle v_2^2 \rangle}$ as the elliptic flow at a given multiplicity, both the PHENIX Collaboration [30] and the STAR Collaboration [31,32] observe

$$v_2\{2\}_{d^{197}\text{Au}} > v_2\{2\}_{p^{197}\text{Au}}.$$

This constitutes a plausible signature of the elliptical geometry of the system formed when a deuterium impinges onto a large gold target. Similarly, at the Large Hadron Collider (LHC) one observes [33–35]

$$v_2\{2\}_{^{208}\text{Pb}^{208}\text{Pb}} > v_2\{2\}_{p^{208}\text{Pb}},$$
$$v_3\{2\}_{^{208}\text{Pb}^{208}\text{Pb}} \approx v_3\{2\}_{p^{208}\text{Pb}}.$$

The enhancement of elliptic flow in $^{208}\text{Pb} + ^{208}\text{Pb}$ collisions is interpreted as coming from the intrinsic ellipticity of the overlap area for off-central collisions, i.e., collisions that are not head-on. These observations hint at the role played by the collision geometry, but employ proton-nucleus collisions as a baseline of a system that does not present any intrinsic shape. This presents two drawbacks. First, proton-nucleus collisions have a different longitudinal structure than nucleus-nucleus collisions (including $d^{197}\text{Au}$ collisions [36,37]), whose geometry is better correlated across rapidities [38,39]. Second, the geometry of proton-nucleus collisions largely depends on the proton structure at low values of the Bjorken x variable, which is poorly understood [7]. Thus, it would be desirable to isolate signatures of the geometry of the initial states in the scattering of actual ions, presenting a well-defined notion of an interaction region.

Upcoming data on collisions of ^{16}O isotopes are expected to mitigate these issues [40]. Preliminary data from $^{16}\text{O} + ^{16}\text{O}$ collisions were recently presented at the Quark Matter 2023 conference by the STAR Collaboration [41]. At the CERN LHC, a run of $^{16}\text{O} + ^{16}\text{O}$ collisions is expected to take place in 2025. Comparing peripheral $^{208}\text{Pb} + ^{208}\text{Pb}$ (or $^{129}\text{Xe} + ^{129}\text{Xe}$) collisions and central $^{16}\text{O} + ^{16}\text{O}$ collisions should reveal [42–44]

$$v_2\{2\}_{^{208}\text{Pb}^{208}\text{Pb}} > v_2\{2\}_{^{16}\text{O}^{16}\text{O}}.$$

However, this comparison is suboptimal. Peripheral $^{208}\text{Pb} + ^{208}\text{Pb}$ collisions have a highly elongated geometry on average, whereas ultracentral $^{16}\text{O} + ^{16}\text{O}$ collisions are dominated by fluctuations. The longitudinal structure of these initial states is different, making a quantitative understanding of these results more challenging.

In this Letter, we demonstrate an alternative more robust approach to isolate the impact of the initial-state geometry. We study central collisions of light ions presenting different shapes. Differences in the collective flow between two collision systems would demonstrate the influence of the nuclear geometry, a technique akin to that used to infer nuclear deformation effects in isobar collisions at RHIC [45–48]. The advantage with light species is that we benefit from an advanced knowledge of their geometries coming from *ab initio* calculations of nuclear structure [49,50]. The drawback with light-ion collisions is instead that the anisotropy induced by nuclear shapes is only a small correction to the anisotropy induced by large density fluctuations caused by the small number of participant nucleons. In other words, with light ions extreme nuclear shapes are required for their fingerprints to be detectable in the final state.

Here, we overcome this issue. We exploit the fact that the stable isotope presenting the most extreme ground-state geometry in the Segrè chart, namely, ^{20}Ne, is close in mass to ^{16}O. We argue that having $^{20}\mathrm{Ne}+{}^{20}\mathrm{Ne}$ data in conjunction with $^{16}\mathrm{O}+{}^{16}\mathrm{O}$ data leads to the observation of unambiguous imprints of the initial-state geometry on the collective flow. This will set a new benchmark for hydrodynamic models at system sizes corresponding to high-multiplicity $\mathrm{p}+{}^{208}\mathrm{Pb}$ collisions that will be crucial for advancing the interpretation of small-system data.

Nuclear structure inputs—Modern *ab initio* approaches to the nuclear many-body problem aim at solving as exactly as possible Schrödinger's equation for nuclear Hamiltonians constructed through chiral effective field theories of low-energy QCD. Such approaches are routinely used to describe the structure of light- and medium-mass nuclei [51–56] and first applications to ^{208}Pb were even recently reported [56,57]. In this work, we employ results for the structure of ^{16}O and ^{20}Ne derived within the framework of nuclear lattice effective field theory (NLEFT) simulations and the *ab initio* projected generator coordinate method (PGCM).

The NLEFT framework [58–60] combines the principles of effective field theory with lattice Monte Carlo methods, and is well suited to probe clustering and other collective phenomena in the ground states of nuclei [61]. NLEFT simulations implement a Euclidean time evolution coupled with auxiliary-field Monte Carlo simulations to produce ground-state configurations of nucleons for each realization of the nuclear wave function. The pin-hole algorithm [61] enables one to keep track of the positions of the nucleons during the Euclidean time evolution while preserving the information about their center of mass. The produced nuclear configurations carry, thus, many-body correlations to all orders as dictated by the ground state of the Hamiltonian. We employ a minimal pionless EFT Hamiltonian with a periodic lattice of eight sites with spacing $a = 1.315$ fm [62], which successfully reproduces measured binding energies and charge radii for the isotopes under study. For ^{16}O, the pinhole configurations are taken from Ref. [63], while a new set is calculated for ^{20}Ne. Because of the larger mass number, these configurations contain a larger fraction of nuclei with a nonunique center of mass due to the periodicity, as well as a higher number of negative-weight states [59,61] than the ^{16}O ones. These issues are addressed in the evaluation of our uncertainties for the subsequent hydrodynamic study [see Supplemental Material (SM)] [64]. Lastly, we distribute nucleons at each lattice site uniformly between $-a/2$ and $a/2$ while maintaining a minimum internucleon distance, d_{min}, to mimic the effect of short-range repulsion.

The *ab initio* PGCM formalism [65–70] is also adapted to describe collective correlations, e.g., quadrupolar and octupolar deformations that appear in doubly-open-shell systems such as ^{20}Ne. In particular, it was shown in Ref. [69] that this method captures experimental data on the ground-state rotational band and the charge density of this nucleus, employing a recent N^{3}LO chiral EFT Hamiltonian [71] which we also use here. We first perform PGCM calculations exploring simultaneously the triaxial quadrupole $(\beta^v_{20}, \beta^v_{22})$ and octupole $(\beta^v_{30}, \beta^v_{32})$ degrees of freedom to determine average intrinsic deformations for the correlated ground states of ^{16}O and ^{20}Ne. The resulting shape parameters align with the results of empirical frameworks such as the energy density functional approach [72–74] or the antisymmetrized molecular dynamics approach [75]. Then, we compute an intrinsic Hartree-Fock-Bogoliubov state constrained at those average deformations, and we evaluate the particle-number projected one-body density of the resulting system. To quantify the systematic uncertainty on the procedure, the average deformations of the ground states are computed from pure mean-field states as well as from particle-number-projected states (more details in SM). The results in the latter case are shown in Fig. 1. We note deformed geometries with well-separated clusters. In ^{16}O they form an irregular tetrahedron with two short and two long edges of 2.30 and 2.55 fm, respectively (see Ref. [76] for recent work employing a regular tetrahedron). For ^{20}Ne we observe a characteristic bowling-pin-like $^{16}\mathrm{O}+\alpha$.

For the hydrodynamic simulations, the densities in Fig. 1 are randomly oriented and used to sample either 16 or 20 coordinates of nucleons for each realization of the nucleus. Unlike the NLEFT simulations, PGCM does not provide us with correlated samplings of nucleon positions. Sampling nucleons capturing the ground-state correlations of the N^{3}LO Hamiltonian is therefore ambiguous. We use two methods as a quantification of this systematic uncertainty. One samples nucleons independently (as in [77,78]), whereas the second divides up space into four or five regions (see Fig. 1) and samples exactly two protons and two neutrons from each (see also SM). Lastly, configurations are rejected if nucleons are closer than d_{min}.

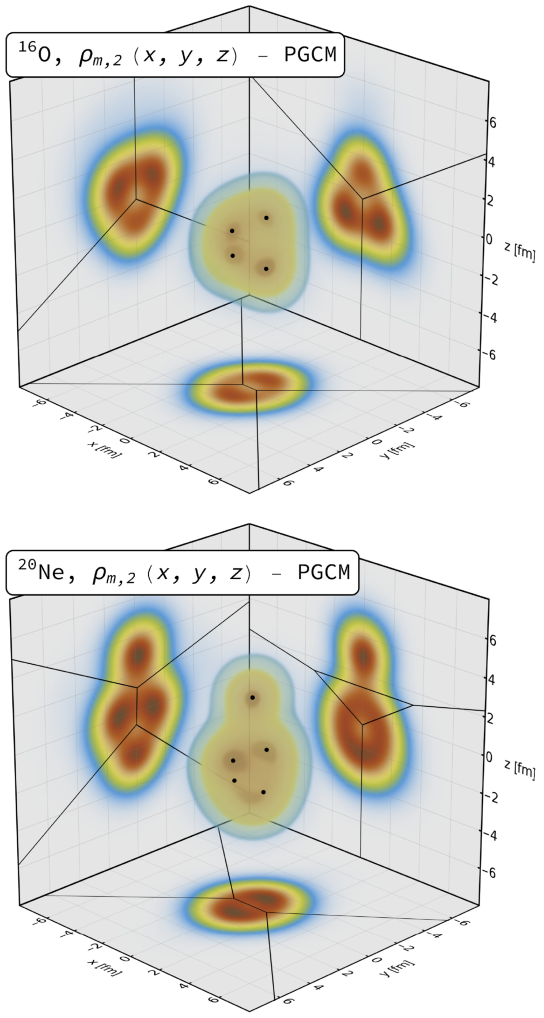

FIG. 1. Point-nucleon densities of ^{16}O and ^{20}Ne obtained from particle-number-projected Hartree-Fock-Bogoliubov states with deformations constrained to the predictions of the *ab initio* PGCM framework. The background plots show slices of the densities through the origin. The black dots and lines show the centers and boundaries of the regions used in the clustered sampling method (see text and SM for details).

Hydrodynamic simulations—We perform event-by-event hydrodynamic simulations of ^{20}Ne + ^{20}Ne and ^{16}O + ^{16}O collisions by means of the Trajectum framework [44,79–81]. The calculations start with configurations of nucleons in the colliding nuclei, taken from either the PGCM or the NLEFT results [82]. Each collision is then assigned to an impact parameter, participant nucleons are selected, and energy density is deposited in the transverse plane. Following a brief pre-equilibrium phase, the system is evolved as a relativistic viscous fluid. Hydrodynamic cooling lasts until the local temperature reaches a critical value ($T \sim 154$ MeV), below which hadronization occurs. Subsequent strong decays and rescattering of hadrons are computed by the SMASH code [83–85], leading to the particle distributions in the final state. These are analyzed to construct multiparticle correlations following the experimental protocols. We define the collision centrality from the multiplicity of charged particles with $p_T \geq 0.4$ GeV and $|\eta| \leq 2.4$, with 0% centrality corresponding to the limit of small impact parameters.

The parameters of the model are chosen probabilistically by sampling from the posterior distribution inferred in a Bayesian analysis of ^{208}Pb + ^{208}Pb collisions, within the same model [86]. We use twenty different samples from the parameter space to quantify the uncertainty on the results coming from wide parameter variations. This represents the largest part of the Trajectum systematic uncertainty, which in addition also takes into account effects of finite grid spacing (as discussed in SM).

Our results for p_T-integrated observables that characterize the collective flow of hadrons are displayed in Fig. 2. Our first remark concerns the cancellation of uncertainties we observe when a relative variation of observables, e.g., a ratio, is taken between ^{16}O + ^{16}O and ^{20}Ne + ^{20}Ne collisions. The dominant uncertainty on the absolute magnitude of the results (upper two plots in each panel) is the systematic one. However, in the relative variations (lowest plots) the contribution from the systematic error becomes nearly equal to that from the statistical error. This enables us to make robust predictions for percent-level variations of observables across the two systems. As discussed in SM, the larger uncertainty affecting the PGCM results is due to the ambiguities of the empirical method used to extract the correlated distributions of nucleons. The systematic uncertainty coming from the NLEFT simulations includes as well the impact of systematic variations of the low-energy constants of the pionless EFT.

We discuss now those observables that are more strongly impacted by the bowling-pin shape of ^{20}Ne. The first is the rms elliptic flow, $v_2\{2\}$, in the lower-left panel of Fig. 2. We find

$$\frac{v_2\{2\}_{\mathrm{NeNe}}}{v_2\{2\}_{\mathrm{OO}}} = \begin{cases} 1.174(8)_{\mathrm{stat}}(31)^{Traj}_{\mathrm{syst}}(4)^{\mathrm{str}}_{\mathrm{syst}} & (\mathrm{NLEFT}), \\ 1.139(6)_{\mathrm{stat}}(27)^{Traj}_{\mathrm{syst}}(28)^{\mathrm{str}}_{\mathrm{syst}} & (\mathrm{PGCM}), \end{cases}$$

in the 0%–1% most central events. This is nearly identical for both nuclear structure inputs, implying that the enhancement of fluctuations in the second harmonic predicted by the NLEFT simulations for ^{20}Ne + ^{20}Ne collisions is largely captured by the (randomly oriented) bowling pin predicted by the PGCM calculation. The $v_2\{2\}$ ratio between ^{20}Ne + ^{20}Ne and ^{16}O + ^{16}O collisions is as large as that expected between peripheral (∼60% off-central) ^{208}Pb + ^{208}Pb collisions and central ^{16}O + ^{16}O collisions [43,44]. However, the cancellation of uncertainties that we achieve here is only possible because we consider experiments with two ions close in mass. We stress that this includes uncertainties related to the detailed modeling of subnucleonic structures, effectively validating

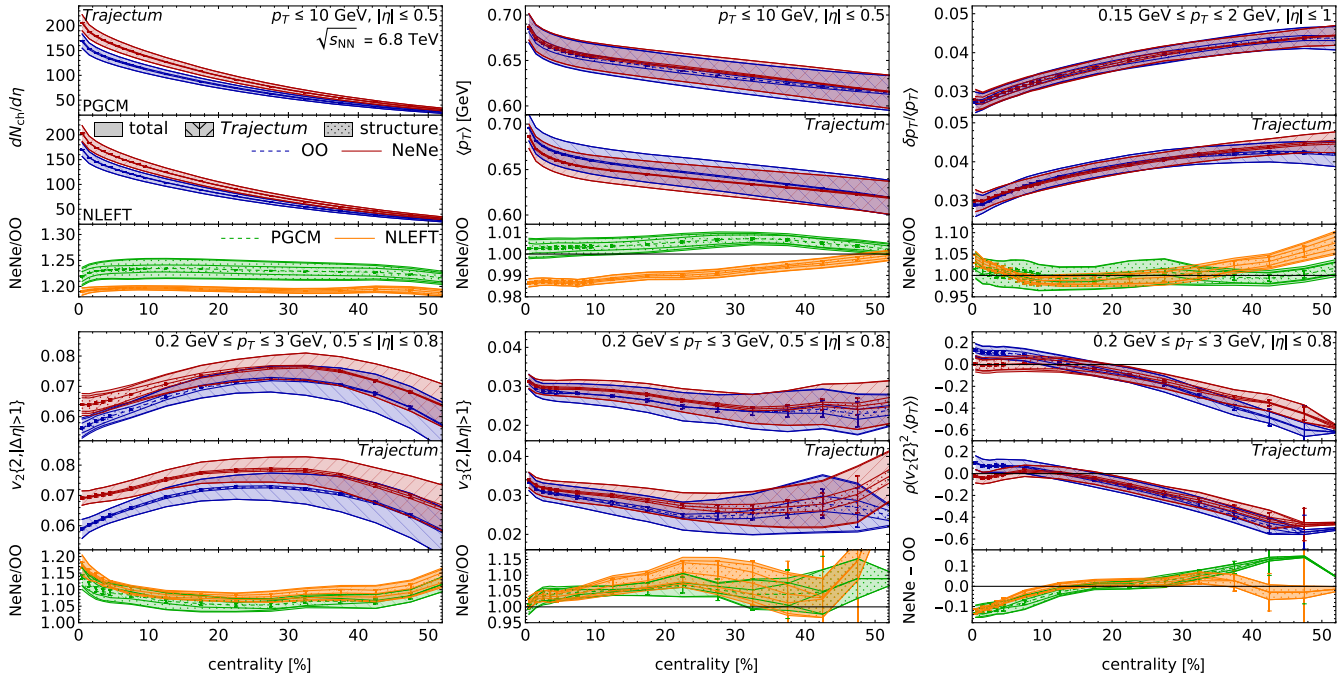

FIG. 2. The deformed shape of ^{20}Ne impacts the hydrodynamic flow of its collisions as compared to ^{16}O + ^{16}O collisions. Here we show results for charged particle multiplicity $dN_{\rm ch}/d\eta$ (top left), mean transverse momentum $\langle p_T \rangle$ (top middle), relative fluctuations of transverse momentum $\delta p_T/\langle p_T \rangle$ (top right), elliptic flow $v_2\{2, |\Delta\eta| > 1\}$ (bottom left), triangular flow $v_3\{2, |\Delta\eta| > 1\}$ (bottom middle) and the Pearson correlation coefficient $\rho(v_2\{2\}^2, \langle p_T \rangle)$ (bottom right). In each panel, we show the ^{16}O + ^{16}O and ^{20}Ne + ^{20}Ne results, as well as their ratio, using both PGCM and NLEFT as nuclear structure inputs. For $\rho(v_2\{2\}^2, \langle p_T \rangle)$ a difference is taken instead of a ratio in the lower panel. We show statistical uncertainties (error bars), the total systematic uncertainty (solid bands) as well as its components being *Trajectum* (hatched) and nuclear structure (dotted).

our initial arguments that comparing light-ion collision systems helps reduce errors related to poorly known features of the high-energy nucleon structure.

Another probe of the bowling-pin shape of ^{20}Ne is the correlation between the mean squared elliptic flow, $v_2\{2\}^2$, and the mean transverse momentum, $\langle p_T \rangle$. It is quantified via a Pearson coefficient denoted by $\rho_2 \equiv \rho(v_2\{2\}^2, \langle p_T \rangle)$ [87], which reflects the correlation between the shape and the size of the produced QGP droplets [43,88,89]. Results for ρ_2 are reported in the lower-right panel of Fig. 2. The suppression of the observable in central ^{20}Ne + ^{20}Ne collisions relative to ^{16}O + ^{16}O, observed for both nuclear structure inputs, is a generic signature of the elongated nuclear shape [77,90–93]. The same effect has been reported in ^{238}U + ^{238}U [94] and ^{129}Xe + ^{129}Xe [95,96] experiments.

The ρ_2 correlator is strongly sensitive to several hydrodynamic model parameters, and thus plagued by a large systematic uncertainty which makes ^{16}O + ^{16}O and ^{20}Ne + ^{20}Ne results overlap. Neglecting the triaxiality of these nuclei, and dubbing β_2 the nuclear quadrupole deformation (where $\beta_{2,^{20}\mathrm{Ne}} > \beta_{2,^{16}\mathrm{O}}$ from spectroscopic data [97], as well as from the densities shown in Fig. 1), the ρ_2 observable roughly follows at a given centrality: $\rho_2 = a - b\beta_2^3$, where a and b are positive coefficients [94,98,99]. Model studies suggest that both a and b are nearly independent of the collision system at the same centrality [77,98]. As a consequence, we expect the difference $\rho_{2,\mathrm{Ne+Ne}} - \rho_{2,\mathrm{O+O}} \propto \left(\beta^3_{2,^{16}\mathrm{O}} - \beta^3_{2,^{20}\mathrm{Ne}}\right)$ to isolate the imprint of the nuclear deformation. This is confirmed in Fig. 2 (lower-right panel), where the evaluated difference cancels most of the systematic uncertainties. A comment is in order. In hydrodynamics, the ρ_2 of ultracentral ^{16}O + ^{16}O collisions is about the same as that of peripheral ^{208}Pb + ^{208}Pb collisions at the same multiplicities [81,100]. Therefore, contrary to the enhancement of $v_2\{2\}$ relative to ^{16}O + ^{16}O systems, which occurs in both central ^{20}Ne + ^{20}Ne and peripheral ^{208}Pb + ^{208}Pb collisions, the suppression of ρ_2 represents a geometry-driven effect only accessible by colliding ^{20}Ne isotopes.

Four more observables are in Fig. 2, namely, the charged multiplicity, $dN_{\rm ch}/d\eta$, the mean transverse momentum, $\langle p_T \rangle$, the fluctuations thereof, and the triangular flow, $v_3\{2\}$. Significant differences appear between PGCM and NLEFT for $dN_{\rm ch}/d\eta$ and $\langle p_T \rangle$ in the ratio plots. These can be understood from the respective nuclear radii [101]. The NLEFT charge rms radii are 2.76 and 3.17 fm for ^{16}O and ^{20}Ne, respectively, (ratio 1.14), whereas clustered PGCM has 2.87 and 3.09 fm with ratio 1.08. For both NLEFT and PGCM we use a Gaussian nucleon charge

distribution of width 0.84 fm [102,103]. This compares well with the experimental values 2.6955 and 3.0055 fm (ratio 1.11) [104]. We note that for PGCM the independent sampling method gives 0.05 and 0.03 fm smaller radii for ^{16}O and ^{20}Ne, respectively. The d_{min} parameter has negligible effect when smaller than 0.5 fm, but increases especially the PGCM radii for larger values. Because of the relatively larger difference in size comparing ^{20}Ne and ^{16}O, the NLEFT results lead to a smaller $\langle p_T \rangle$ for $^{20}\mathrm{Ne} + {}^{20}\mathrm{Ne}$ as compared to the PGCM results due to a reduced radial expansion. Similarly, the larger size of the PGCM oxygen leads to an increased $^{16}\mathrm{O} + {}^{16}\mathrm{O}$ cross section and consequently per collision a lower multiplicity, affecting the $dN_{\mathrm{ch}}/d\eta$ ratio (see also Ref. [86]). For the fluctuations of $\langle p_T \rangle$ the observed mild enhancement in central $^{20}\mathrm{Ne} + {}^{20}\mathrm{Ne}$ collisions is a generic consequence of the more deformed ^{20}Ne shape, which enhances fluctuations in the overall size of the overlap region [98,105].

Conclusion and outlook—We have showcased the possibility of reducing theoretical systematic uncertainties in hydrodynamic model calculations of small systems. One needs experiments with two light-ion species presenting sufficiently different geometries. Interaction dynamics in the region of nuclear overlap leads, then, to nuclear-shape-induced modifications of the collective flow, enabling one to perform quantitative tests of the QGP paradigm. As $^{16}\mathrm{O} + {}^{16}\mathrm{O}$ collisions are essentially already available at colliders, the extreme shape of ^{20}Ne makes this proposal realizable in practice.

Our predictions are based on the same hydrodynamic picture used in the description of collisions of heavy nuclei. They do not include additional ingredients, e.g., out-of-equilibrium corrections due to the expected partial thermalization of the interaction region [23,106,107], the breakdown of the equations used in our simulations due to causality constraints [108–110], features such as the escape mechanism [111] that would affect the elliptic flow in a transport-based approach, or even the impact of momentum anisotropies originating in the initial states [24]. Therefore, testing our predictions in experiments will provide unprecedented quantitative insights into the applicability of a QGP paradigm and the emergence of collective dynamics in QCD matter.

As an outlook, additional research avenues are opened by the study of high-energy $^{20}\mathrm{Ne} + {}^{20}\mathrm{Ne}$ collisions. They will be the subject of future works.

The elongated ^{20}Ne shape may help reveal hard-probe modifications in a small system via the study of path-length-dependent effects in the comparison between $^{20}\mathrm{Ne} + {}^{20}\mathrm{Ne}$ and $^{16}\mathrm{O} + {}^{16}\mathrm{O}$ collisions. These can be studied experimentally by triggering on ultracentral events presenting large final-state ellipticities [112], and estimated theoretically from the analysis of the path lengths traversed by the hard probes [113].

Second, both ^{16}O and ^{20}Ne can be injected in the SMOG2 system of the LHCb detector to perform fixed-target experiments at $\sqrt{s_{\mathrm{NN}}} \approx 0.07$ TeV in the center-of-mass frame [114]. The LHC could thus deliver $^{20}\mathrm{Ne} + {}^{20}\mathrm{Ne}$ and $^{16}\mathrm{O} + {}^{16}\mathrm{O}$ collisions at both $\sqrt{s_{\mathrm{NN}}} \approx 7$ and 0.07 TeV, as well as fixed-target $^{20}\mathrm{Ne} + {}^{208}\mathrm{Pb}$ and $^{16}\mathrm{O} + {}^{208}\mathrm{Pb}$ collisions. This wealth of experimental information combined with the possibility of canceling uncertainties via the study of relative observables would provide a unique handle on the manifestations of small-x dynamics and nonlinear QCD evolution and how they impact the collective structure of nuclei [115].

Finally, several γ-mediated processes in ultraperipheral nucleus-nucleus collisions (UPCs) are aimed at imaging the gluonic content of nuclei at high energy. As showcased in Ref. [116] for the diffractive production of J/ψ, the shape of ^{20}Ne can leave distinct signatures on the cross sections on top of a $\gamma + {}^{16}\mathrm{O}$ background. Ratios of observables in UPCs would allow one to cancel uncertainties and obtain a more transparent view of the gluon geometries and their modification at high energy.

Acknowledgments—We acknowledge the participants of the EMMI Rapid Reaction Task Force "Nuclear physics confronts relativistic collisions of isobars" and of the ESNT workshop "Deciphering nuclear phenomenology across energy scales" for fruitful discussions about the applications of ^{20}Ne, that have triggered this project. G. G. is funded by the Deutsche Forschungsgemeinschaft (DFG, German Research Foundation) (German Research Foundation)—Project-ID 273811115—SFB 1225 ISOQUANT, and under Germany's Excellence Strategy EXC2181/1-390900948 (the Heidelberg STRUCTURES Excellence Cluster). We also acknowledge support from the U.S. Department of Energy (DE-SC0024586, DE-SC0023658, DE-SC0013365, DE-SC0023175) and the U.S. National Science Foundation (PHY-2310620). This work is supported in part by the European Research Council (ERC) under the European Union's Horizon 2020 research and innovation programme (ERC AdG EXOTIC, Grant Agreement No. 101018170), by DFG and NSFC through funds provided to the Sino-German CRC 110 "Symmetries and the Emergence of Structure in QCD" (NSFC Grant No. 11621131001, DFG Grant No. TRR110). The work of U.-G. M. was supported in part by the CAS President's International Fellowship Initiative (PIFI) (Grant No. 2018DM0034). R. R. is supported by the Deutsche Forschungsgemeinschaft (DFG, German Research Foundation)—Projektnummer 279384907—SFB 1245. T. R. R. is supported by the Spanish MCIU (PID2021- 127890NB-I00). The PGCM calculations were performed using HPC resources from GENCI-TGCC (Contracts No. A0130513012 and No. A0150513012) and CCRT (TOPAZE supercomputer). The NLEFT code development and production calculations

utilized the following computational resources: the Gauss Centre for Supercomputing e.V. [117] for computing time on the GCS Supercomputer JUWELS at Jülich Supercomputing Centre (JSC) and special GPU time allocated on JURECA-DC; the Oak Ridge Leadership Computing Facility through the INCITE award "*Ab-initio* nuclear structure and nuclear reactions"; and the TUBITAK ULAKBIM High Performance and Grid Computing Center (TRUBA resources). J. N. H. acknowledges financial support from the US-DOE Nuclear Science Grant No. DE-SC0023861 and within the framework of the Saturated Glue (SURGE) Topical Theory.

[1] W. Busza, K. Rajagopal, and W. van der Schee, Annu. Rev. Nucl. Part. Sci. **68**, 339 (2018).
[2] D. A. Teaney,Viscous hydrodynamics and the quark gluon plasma, in *Quark-Gluon Plasma 4*, edited by R. C. Hwa and X.-N. Wang (World Scientific, Singapore, 2010), pp. 207–266, 10.1142/9789814293297_0004.
[3] J.-Y. Ollitrault, Eur. Phys. J. A **59**, 236 (2023).
[4] J.-Y. Ollitrault, Phys. Rev. D **46**, 229 (1992).
[5] D. Teaney and L. Yan, Phys. Rev. C **83**, 064904 (2011).
[6] J. L. Nagle and W. A. Zajc, Annu. Rev. Nucl. Part. Sci. **68**, 211 (2018).
[7] B. Schenke, Rept. Prog. Phys. **84**, 082301 (2021).
[8] J. Noronha, B. Schenke, C. Shen, and W. Zhao, Int. J. Mod. Phys. E **33**, 2430005 (2024).
[9] G. S. Rocha, D. Wagner, G. S. Denicol, J. Noronha, and D. H. Rischke, Entropy **26**, 189 (2024).
[10] R. D. Weller and P. Romatschke, Phys. Lett. B **774**, 351 (2017).
[11] H. Mäntysaari, B. Schenke, C. Shen, and P. Tribedy, Phys. Lett. B **772**, 681 (2017).
[12] J. S. Moreland, J. E. Bernhard, and S. A. Bass, Phys. Rev. C **101**, 024911 (2020).
[13] B. Schenke, C. Shen, and P. Tribedy, Phys. Lett. B **803**, 135322 (2020).
[14] W. Zhao, Y. Zhou, K. Murase, and H. Song, Eur. Phys. J. C **80**, 846 (2020).
[15] Y. Wang, W. Zhao, and H. Song, arXiv:2401.00913.
[16] A. Kurkela, U. A. Wiedemann, and B. Wu, Phys. Lett. B **783**, 274 (2018).
[17] A. Kurkela, U. A. Wiedemann, and B. Wu, Eur. Phys. J. C **79**, 759 (2019).
[18] A. Kurkela, A. Mazeliauskas, J.-F. Paquet, S. Schlichting, and D. Teaney, Phys. Rev. Lett. **122**, 122302 (2019).
[19] A. Kurkela, U. A. Wiedemann, and B. Wu, Eur. Phys. J. C **79**, 965 (2019).
[20] A. Kurkela, S. F. Taghavi, U. A. Wiedemann, and B. Wu, Phys. Lett. B **811**, 135901 (2020).
[21] V. E. Ambrus, S. Schlichting, and C. Werthmann, Phys. Rev. D **105**, 014031 (2022).
[22] V. E. Ambrus, S. Schlichting, and C. Werthmann, Phys. Rev. D **107**, 094013 (2023).
[23] V. E. Ambrus, S. Schlichting, and C. Werthmann, Phys. Rev. Lett. **130**, 152301 (2023).
[24] T. Altinoluk and N. Armesto, Eur. Phys. J. A **56**, 215 (2020).
[25] P. Romatschke and U. Romatschke, *Relativistic Fluid Dynamics in and out of Equilibrium*, Cambridge Monographs on Mathematical Physics (Cambridge University Press, Cambridge, England, 2019), http://dx.doi.org/10.1017/9781108651998.
[26] J.-P. Blaizot and L. Yan, Ann. Phys. (Amsterdam) **412**, 167993 (2020).
[27] S. Schlichting and D. Teaney, Annu. Rev. Nucl. Part. Sci. **69**, 447 (2019).
[28] J. Berges, M. P. Heller, A. Mazeliauskas, and R. Venugopalan, Rev. Mod. Phys. **93**, 035003 (2021).
[29] A. Soloviev, Eur. Phys. J. C **82**, 319 (2022).
[30] C. Aidala *et al.* (PHENIX Collaboration), Nat. Phys. **15**, 214 (2019).
[31] M. I. Abdulhamid *et al.* (STAR Collaboration), Phys. Rev. Lett. **130**, 242301 (2023).
[32] M. I. Abdulhamid, B. E. Aboona, J. Adam, J. R. Adams, G. Agakishiev, I. Aggarwal, M. M. Aggarwal, Z. Ahammed, A. Aitbaev *et al.*, Phys. Rev. C **110**, 064902 (2024).
[33] S. Chatrchyan *et al.* (CMS Collaboration), Phys. Lett. B **724**, 213 (2013).
[34] M. Aaboud *et al.* (ATLAS Collaboration), Eur. Phys. J. C **77**, 428 (2017).
[35] S. Acharya *et al.* (ALICE Collaboration), Phys. Rev. Lett. **123**, 142301 (2019).
[36] U. A. Acharya *et al.* (PHENIX Collaboration), Phys. Rev. C **105**, 024901 (2022).
[37] W. Zhao, S. Ryu, C. Shen, and B. Schenke, Phys. Rev. C **107**, 014904 (2023).
[38] V. Khachatryan *et al.* (CMS Collaboration), Phys. Rev. C **92**, 034911 (2015).
[39] P. Bozek and W. Broniowski, Phys. Lett. B **752**, 206 (2016).
[40] J. Brewer, A. Mazeliauskas, and W. van der Schee, in Proceedings of the Opportunities of OO and pO collisions at the LHC (2021), arXiv:2103.01939.
[41] S. Huang, arXiv:2312.12167.
[42] M. D. Sievert and J. Noronha-Hostler, Phys. Rev. C **100**, 024904 (2019).
[43] B. Schenke, C. Shen, and P. Tribedy, Phys. Rev. C **102**, 044905 (2020).
[44] G. Nijs and W. van der Schee, Phys. Rev. C **106**, 044903 (2022).
[45] G. Giacalone, J. Jia, and V. Somà, Phys. Rev. C **104**, L041903 (2021).
[46] M. Abdallah *et al.* (STAR Collaboration), Phys. Rev. C **105**, 014901 (2022).
[47] C. Zhang and J. Jia, Phys. Rev. Lett. **128**, 022301 (2022).
[48] G. Nijs and W. van der Schee, SciPost Phys. **15**, 041 (2023).
[49] H. Hergert, Front. Phys. **8**, 379 (2020).
[50] A. Ekström, C. Forssén, G. Hagen, G. R. Jansen, W. Jiang, and T. Papenbrock, Front. Phys. **11**, 1129094 (2023).
[51] G. Hagen, T. Papenbrock, M. Hjorth-Jensen, and D. J. Dean, Rep. Prog. Phys. **77**, 096302 (2014).
[52] H. Hergert, S. K. Bogner, T. D. Morris, A. Schwenk, and K. Tsukiyama, Phys. Rep. **621**, 165 (2016).
[53] V. Somà, P. Navrátil, F. Raimondi, C. Barbieri, and T. Duguet, Phys. Rev. C **101**, 014318 (2020).

[54] S. R. Stroberg, J. D. Holt, A. Schwenk, and J. Simonis, Phys. Rev. Lett. **126**, 022501 (2021).
[55] A. Tichai, R. Roth, and T. Duguet, Front. Phys. **8**, 164 (2020).
[56] P. Arthuis, K. Hebeler, and A. Schwenk, arXiv:2401.06675.
[57] B. Hu *et al.*, Nat. Phys. **18**, 1196 (2022).
[58] D. Lee, Prog. Part. Nucl. Phys. **63**, 117 (2009).
[59] T. A. Lähde and U.-G. Meißner, *Nuclear Lattice Effective Field Theory: An Introduction* (Springer, New York, 2019), Vol. 957.
[60] D. Lee, Front. Phys. **8**, 174 (2020).
[61] S. Elhatisari, E. Epelbaum, H. Krebs, T. A. Lähde, D. Lee, N. Li, B.-n. Lu, U.-G. Meißner, and G. Rupak, Phys. Rev. Lett. **119**, 222505 (2017).
[62] B.-N. Lu, N. Li, S. Elhatisari, D. Lee, E. Epelbaum, and U.-G. Meißner, Phys. Lett. B **797**, 134863 (2019).
[63] N. Summerfield, B.-N. Lu, C. Plumberg, D. Lee, J. Noronha-Hostler, and A. Timmins, Phys. Rev. C **104**, L041901 (2021).
[64] See Supplemental Material at http://link.aps.org/supplemental/10.1103/k8rb-jgvq for a detailed discussion of the treatment of uncertainties.
[65] M. Frosini, T. Duguet, B. Bally, Y. Beaujeault-Taudière, J. P. Ebran, and V. Somà, Eur. Phys. J. A **57**, 151 (2021).
[66] J. M. Yao, J. Engel, L. J. Wang, C. F. Jiao, and H. Hergert, Phys. Rev. C **98**, 054311 (2018).
[67] J. M. Yao, B. Bally, J. Engel, R. Wirth, T. R. Rodríguez, and H. Hergert, Phys. Rev. Lett. **124**, 232501 (2020).
[68] M. Frosini, T. Duguet, J.-P. Ebran, and V. Somà, Eur. Phys. J. A **58**, 62 (2022).
[69] M. Frosini, T. Duguet, J.-P. Ebran, B. Bally, T. Mongelli, T. R. Rodríguez, R. Roth, and V. Somà, Eur. Phys. J. A **58**, 63 (2022).
[70] M. Frosini, T. Duguet, J.-P. Ebran, B. Bally, H. Hergert, T. R. Rodríguez, R. Roth, J. Yao, and V. Somà, Eur. Phys. J. A **58**, 64 (2022).
[71] T. Hüther, K. Vobig, K. Hebeler, R. Machleidt, and R. Roth, Phys. Lett. B **808**, 135651 (2020).
[72] S. Marcos, H. Flocard, and P. H. Heenen, Nucl. Phys. **A410**, 125 (1983).
[73] L. M. Robledo and G. F. Bertsch, Phys. Rev. C **84**, 054302 (2011).
[74] P. Marević, J. P. Ebran, E. Khan, T. Nikšić, and D. Vretenar, Phys. Rev. C **97**, 024334 (2018).
[75] M. Kimura, T. Suhara, and Y. Kanada-En'yo, Eur. Phys. J. A **52**, 373 (2016).
[76] Y. Wang, S. Zhao, B. Cao, H.-j. Xu, and H. Song, Phys. Rev. C **109**, L051904 (2024).
[77] B. Bally, M. Bender, G. Giacalone, and V. Somà, Phys. Rev. Lett. **128**, 082301 (2022).
[78] B. Bally, G. Giacalone, and M. Bender, Eur. Phys. J. A **58**, 187 (2022).
[79] G. Nijs, W. van der Schee, U. Gürsoy, and R. Snellings, Phys. Rev. Lett. **126**, 202301 (2021).
[80] G. Nijs, W. van der Schee, U. Gürsoy, and R. Snellings, Phys. Rev. C **103**, 054909 (2021).
[81] G. Nijs and W. van der Schee, Phys. Rev. Lett. **129**, 232301 (2022).
[82] For all profiles we provide 20 k configurations as part of the submission.
[83] J. Weil *et al.* (SMASH Collaboration), Phys. Rev. C **94**, 054905 (2016).
[84] D. Oliinychenko, V. Steinberg, J. Weil, M. Kretz, J. Staudenmaier, S. Ryu, A. Schäfer, J. Rothermel, J. Mohs, F. Li, H. E. (Petersen), L. Pang, D. Mitrovic, A. Goldschmidt, L. Geiger, J.-B. Rose, J. Hammelmann, and L. Prinz, smash-transport/smash: Smash-1.8 (2020).
[85] T. Sjostrand, S. Mrenna, and P. Z. Skands, Comput. Phys. Commun. **178**, 852 (2008).
[86] G. Giacalone, G. Nijs, and W. van der Schee, Phys. Rev. Lett. **131**, 202302 (2023).
[87] P. Bozek, Phys. Rev. C **93**, 044908 (2016).
[88] P. Bozek and H. Mehrabpour, Phys. Rev. C **101**, 064902 (2020).
[89] G. Giacalone, F. G. Gardim, J. Noronha-Hostler, and J.-Y. Ollitrault, Phys. Rev. C **103**, 024909 (2021).
[90] G. Giacalone, Phys. Rev. Lett. **124**, 202301 (2020).
[91] G. Giacalone, Phys. Rev. C **102**, 024901 (2020).
[92] J. Jia, S. Huang, and C. Zhang, Phys. Rev. C **105**, 014906 (2022).
[93] N. Magdy, Eur. Phys. J. A **59**, 64 (2023).
[94] STAR Collaboration, Nature (London) **635**, 67 (2024).
[95] S. Acharya *et al.* (ALICE Collaboration), Phys. Lett. B **834**, 137393 (2022).
[96] G. Aad *et al.* (ATLAS Collaboration), Phys. Rev. C **107**, 054910 (2023).
[97] B. Pritychenko, M. Birch, B. Singh, and M. Horoi, At. Data Nucl. Data Tables **107**, 1 (2016); **114**, 371(E) (2017).
[98] J. Jia, Phys. Rev. C **105**, 044905 (2022).
[99] G. Giacalone, Eur. Phys. J. A **59**, 297 (2023).
[100] G. Giacalone, B. Schenke, and C. Shen, Phys. Rev. Lett. **125**, 192301 (2020).
[101] Here the charge radii equal the matter radii for NLEFT since the computation is isospin symmetric. For PGCM the matter radii are about 0.012 fm smaller than the charge radii.
[102] P. A. Zyla *et al.* (Particle Data Group), Prog. Theor. Exp. Phys. **2020**, 083C01 (2020).
[103] Y.-H. Lin, H.-W. Hammer, and U.-G. Meißner, Phys. Rev. Lett. **128**, 052002 (2022).
[104] I. Angeli and K. P. Marinova, Atom. Data Nucl. Data Tabl. **99**, 69 (2013).
[105] N. Fortier, S. Jeon, and C. Gale, Phys. Rev. C **111**, 014901 (2025).
[106] Y. Kanakubo, Y. Tachibana, and T. Hirano, Phys. Rev. C **105**, 024905 (2022).
[107] Y. Kanakubo, Y. Tachibana, and T. Hirano, Phys. Rev. C **106**, 054908 (2022).
[108] F. S. Bemfica, M. M. Disconzi, V. Hoang, J. Noronha, and M. Radosz, Phys. Rev. Lett. **126**, 222301 (2021).
[109] C. Plumberg, D. Almaalol, T. Dore, J. Noronha, and J. Noronha-Hostler, Phys. Rev. C **105**, L061901 (2022).
[110] R. Krupczak *et al.*, Phys. Rev. C **109**, 034908 (2024).
[111] L. He, T. Edmonds, Z.-W. Lin, F. Liu, D. Molnar, and F. Wang, Phys. Lett. B **753**, 506 (2016).
[112] J. Schukraft, A. Timmins, and S. A. Voloshin, Phys. Lett. B **719**, 394 (2013).
[113] C. Beattie, G. Nijs, M. Sas, and W. van der Schee, Phys. Lett. B **836**, 137596 (2023).

[114] R. Aaij *et al.* (LHCb Collaboration), J. Instrum. **17**, P05009 (2022).
[115] G. Giacalone, B. Schenke, S. Schlichting, and P. Singh, EPJ Web Conf. **296**, 10005 (2024).
[116] H. Mäntysaari, B. Schenke, C. Shen, and W. Zhao, Phys. Rev. Lett. **131**, 062301 (2023).
[117] www.gauss-centre.eu